Clean Energy, 2025, Vol. 9, No. 6, 174–189
https://doi.org/10.1093/ce/zkaf043
Advance access publication 7 August 2025
Research Article

Integrated experimental and computational fluid dynamics study of graphene nanoplatelet-based nanofluids modified with surfactants in photovoltaic-thermal heat exchangers

Saiful Anwar[1], Poppy Puspitasari[1,2,*], Diki Dwi Pramono[1], Avita Ayu Permanasari[1,2], Yahya Zakaria[1] and Mohd Afzanizam Mohd Rosli[3]

[1]Department of Mechanical and Industrial Engineering, Universitas Negeri Malang, Malang 65145, Indonesia
[2]Centre of Advanced Materials and Renewable Energy, Universitas Negeri Malang, Malang 65145, Indonesia
[3]Department of Mechanical Engineering, Universiti Teknikal Malaysia Melaka, Melaka 76100, Malaysia
*Corresponding author. E-mail: poppy@um.ac.id

Abstract

This study investigates the effects of graphene nanoplatelet-based nanofluids, modified with various surfactant types and concentrations, on the thermal performance of solar thermal systems. The nanofluids were synthesized and characterized in terms of structural, thermophysical, rheological, and dispersion properties. These data were integrated into computational simulations of a photovoltaic-thermal heat exchanger. Among all formulations, the nanofluid containing 0.1 wt% polyvinylpyrrolidone exhibited the highest thermal efficiency, increasing from 40.21% (water) to 45.26%. This enhancement is attributed to its superior thermal conductivity, higher specific heat capacity, low viscosity at elevated shear rates, and stable dispersion. Rheological testing confirmed shear-thinning, non-Newtonian behavior that facilitates convective heat transfer. In contrast, nanofluids without surfactants or with anionic surfactants showed higher viscosity and reduced stability, resulting in lower thermal efficiency. The integrated experimental computational approach offers a comprehensive understanding of the mechanisms governing nanofluid-enhanced heat transfer in photovoltaic-thermal systems. Enhancing the heat exchanger directly improves overall system performance. The proposed nanofluid formulation presents a viable pathway toward scalable, efficient solar thermal applications. Future work should focus on long-term stability and techno-economic validation under real-world operating conditions.

Graphical abstract

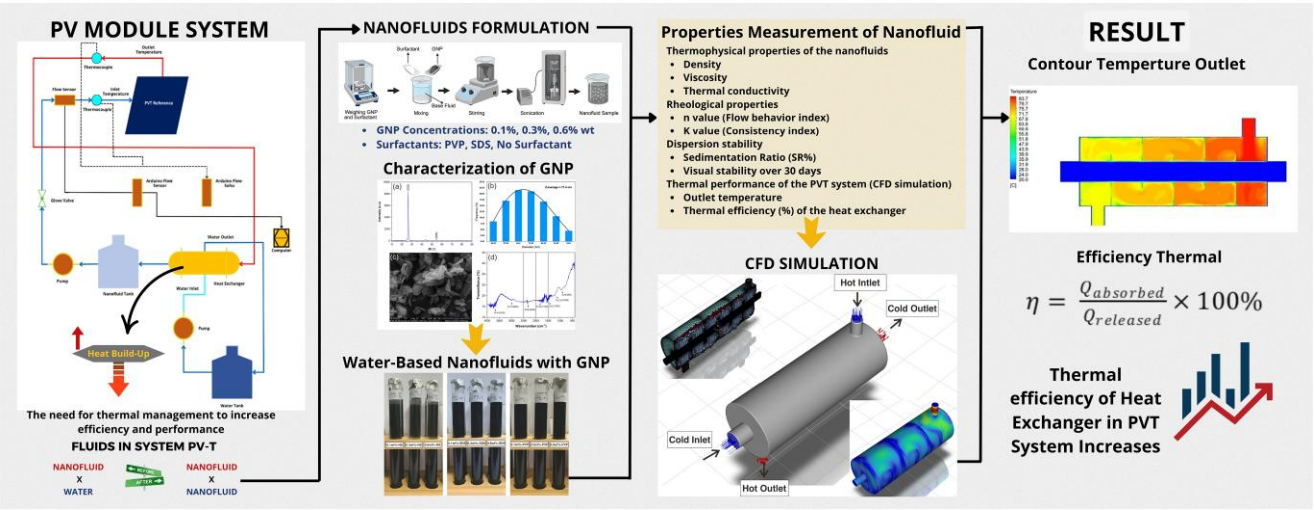

Keywords: graphene nanoplatelet; heat exchanger; nanofluid; photovoltaic-thermal system; rheology; thermal conductivity; thermal efficiency

Received: 6 June 2025. **Accepted:** 5 August 2025

Introduction

Solar energy is widely regarded as a leading renewable source, playing a key role in the global transition to sustainable energy systems [1]. Among the emerging technologies that maximize solar energy utilization is the photovoltaic-thermal (PVT) system, which allows for the simultaneous generation of electricity and thermal energy [2]. However, a key limitation in PVT systems is the temperature rise in photovoltaic (PV) modules, which reduces electrical conversion efficiency by approximately 0.40%–0.50% per 1°C increase [3]. This underscores the urgent need for effective thermal management to maintain energy conversion efficiency.

To address this challenge, nanofluids suspensions of nanoparticles in base fluids have been widely explored for PVT cooling systems [4]. Nanofluids offer enhanced thermophysical properties particularly thermal conductivity and specific heat compared to conventional working fluids. Among the various nanoparticle candidates, graphene nanoplatelets (GNP) stand out due to their high surface area and excellent thermal conductivity [5]. However, surface cooling with nanofluids has been reported to cause uneven flow distribution, fouling, and long-term maintenance issues, limiting its large-scale deployment [6]. Their two-dimensional morphology improves phonon transport, enhancing thermal performance in PVT applications [7]. However, realizing these benefits in practice is contingent upon maintaining nanofluid stability over time.

Stable nanoparticle dispersion is essential for maintaining consistent heat transfer performance [8]. Agglomeration and sedimentation can impair thermal conductivity, increase pressure drop, and potentially block fluid flow [9]. To mitigate this, surfactants such as sodium dodecyl sulfate (SDS) and polyvinylpyrrolidone (PVP) are commonly used. These agents reduce surface tension and form electrostatic or steric barriers that hinder nanoparticle aggregation. Mechanical dispersion with surfactants like sodium dodecylbenzene sulfonate has been proposed to enhance nanoparticle stability [10]. However, their inclusion also alters the fluid's viscosity and density, affecting the overall heat transfer characteristics [11–13]. For instance, while GNP-PVP nanofluids demonstrate improved dispersion stability, they often exhibit increased viscosity and non-Newtonian behavior depending on temperature and shear rate [12]. PVP, in particular, demonstrates superior long-term dispersion stability under thermal cycling, an essential feature for solar thermal applications. However, their practical implementation in PVT systems has not been fully explored, especially in computational fluid dynamic (CFD) models that overlook experimentally derived thermophysical properties [14–16].

Although nanofluids have been widely studied in both experimental and numerical domains, only a few have integrated empirical data such as viscosity, density, and stability into CFD simulations of PVT systems [14]. Recent literature emphasizes the need to consider multivariable interactions in thermal system modeling [15]. Recent reviews underline growing interest in advanced PVT configurations such as integration with vortex generators for flow enhancement, spectral splitters with nanofluid filters, and hybrid PVT-TEG systems [17, 18]. Nevertheless, these studies seldom combine experimental nanofluid characterization with system-level CFD validation, leaving a gap in translating material-level improvements to practical system gains. This gap often limits the practical relevance and optimization of nanofluid-based cooling strategies. Moreover, most existing research isolates variables like nanoparticle type or surfactant effect without considering their combined behavior under dynamic thermal conditions. While GNP-based and hybrid nanofluids are gaining research interest, they remain underrepresented in PVT system optimization [17–19]. As a result, translating material level enhancements into system level performance improvements remains a critical challenge.

To bridge this gap, this study introduces a novel experimental simulation framework integrating the combined effects of surfactant type (SDS, PVP, and no surfactant) and GNP concentration (0.1, 0.3, and 0.6 wt%) on the thermophysical, rheological, and stability characteristics of nanofluids to address real-world application needs. Bridging this methodological disconnect requires a more integrated approach combining experimental validation with performance modeling [20, 21]. To the best of our knowledge, no previous study has systematically validated surfactant-modified GNP nanofluid formulations through both experimental testing and system-level CFD analysis in a single framework. This framework allows better alignment with real-world operational conditions in solar thermal systems, particularly those incorporating reflective, spectral, or thermoelectric modules, as highlighted in recent hybrid PVT research [17, 18, 22]. This dual approach not only offers a comprehensive understanding of surfactant-modified GNP nanofluid behavior. It also provides practical insight into identifying optimal formulations for thermal efficiency in PVT heat exchangers [23].

Novelty

While previous studies have evaluated the use of nanofluids or surfactants separately in PVT systems such as employing bio-based or GNP-based formulations to enhance PV cooling few have integrated both variables into a unified analysis [24, 25]. This study introduces a novel experimental CFD framework that systematically examines the combined influence of GNP concentration (0.1, 0.3, 0.6 wt%) and surfactant type (SDS, PVP, and no surfactant) on nanofluid thermophysical, rheological, and stability characteristics. By incorporating empirically measured parameters directly into a system level PVT heat exchanger simulation, this work enables a more accurate and realistic selection of nanofluid formulations, offering new insight into optimizing thermal performance under actual operating conditions.

Materials and methods

Material

This study utilizes distilled water (aquades) as the base fluid, GNP as the dispersed phase, and surfactants PVP and SDS to enhance dispersion stability. The details of the materials used are presented in Table 1 [25].

Instrument and apparatus

Beaker glass, glass funnel, measuring cylinder, and pycnometer were purchased from Iwaki Glass, Indonesia. The Ultrasonic Horn Labocon LUH-103 from Labocon Scientific Limited, UK. The hotplate magnetic stirrer is from Thermo Fisher Scientific, USA. Digital Weighing Balance Model 2204H with an accuracy of 0.1 mg from WANT Balance Instrument Company, China.

Preparation of GNP nanofluids

The preparation of GNP nanofluids in this study followed a two-step method. As illustrated in Fig. 1. This method involves dispersing presynthesized GNP into a base fluid to create a stable suspension.

Table 1. Materials used in the study.

Name	Category	Function	Supplier/product code	Molecular weight (g/mol)
Aquades	Dispersion medium	Base fluid	—	18.015
GNP	Dispersed phase	Nanoparticle	KNano KNG-150	12.01
PVP	Dispersed phase	Surfactant	Merck 5295-100GM	114.4
SDS	Dispersed phase	Surfactant	Future Chemical CAS:151-21-3	288.38

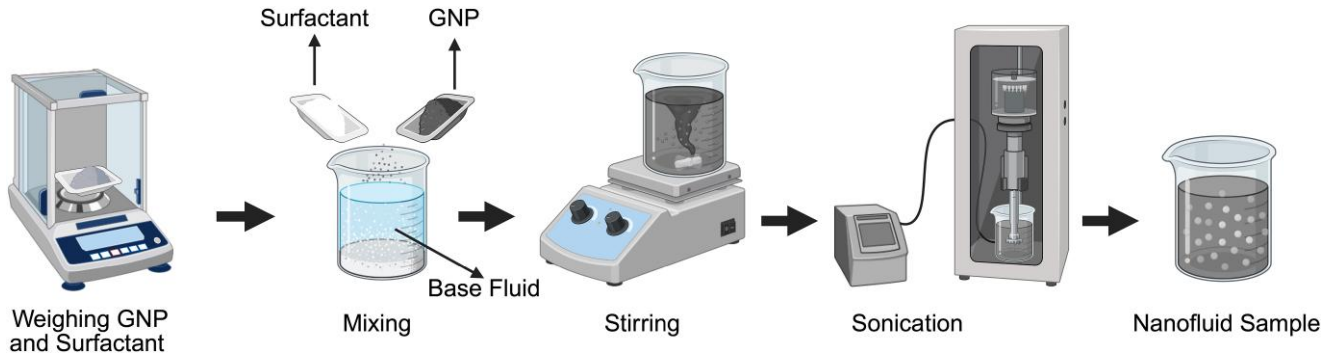

Figure 1. Schematic of nanofluids preparation using GNP. Created in BioRender. Pramono, D. (2025) https://BioRender.com/qsffzvk.

The dispersion process began with magnetic stirring at a speed of 1500 rpm for 15 min to ensure an even distribution of nanoparticles within the fluid [26]. Following this, the mixture underwent sonication for 40 min in 4 sessions 10 min of operation followed by a 5-min break using an ultrasonic device to break down remaining agglomerates and achieve a homogeneous suspension [27]. The combination of magnetic stirring and sonication is essential to achieve optimal dispersion and to prevent sedimentation over time. After preparation, the nanofluid was stored in a sealed container at room temperature to maintain its stability and minimize the risk of agglomeration [28].

The GNP nanoparticles were prepared in three different concentrations (0.1%, 0.3%, and 0.6% by weight) and mixed with distilled water as the base fluid. To enhance the stability of the nanofluids, the surfactants SDS and PVP were added. The surfactant weight percentage used was 40% of the corresponding GNP weight percentage, as shown in Table 2 [26].

Characterization of GNP

Test for phase and crystallite size of GNP

The phase composition and crystallite size of the GNP were analyzed using X-ray diffraction (XRD) [29]. The test was performed at the Laboratory of Minerals and Advanced Materials, Universitas Negeri Malang, employing a PANalytical Expert Pro X-ray diffractometer.

Test for particle size distribution of GNP

The particle size distribution was also measured using a particle size analyzer (PSA) which provided volumetric distribution data of GNP, including the mean particle diameter [30]. This analysis was carried out at the Laboratory Terpadu, Universitas Negeri Malang, employing Size Analyzer Horiba SZ-100.

Test for morphology of GNP

The surface morphology of the GNP was observed using a scanning electron microscope (SEM) [31]. This analysis was carried out at the Laboratory of Minerals and Advanced Materials, Universitas Negeri Malang, with the aid of an FEI Japan Inspect-S50 instrument.

Test for functional groups of GNP

The identification of functional groups in the GNP was performed using Fourier transform infrared (FTIR) spectroscopy. The analysis took place at the Laboratory of Minerals and Advanced Materials, Universitas Negeri Malang, employing a Shimadzu IR Prestige 21 spectrometer [32].

Properties measurement of GNP nanofluid

Test for density of GNP nanofluid

The density measurement was carried out at a standard test temperature of 30°C, 40 °C, and 50°C. The mass was determined using a digital analytical balance, and the volume was measured with a 25 ml pycnometer [33].

The density of nanofluids was estimated using Equation (1) [34].

$$\rho = m/v \tag{1}$$

Test for thermal conductivity of GNP nanofluid

Thermal conductivity testing was conducted to evaluate the ability of GNP to enhance heat transfer in the nanofluid. Measurements were performed at a standard temperature of 40°C using a thermal conductivity analyzer (KD2 Pro from Decagon Devices, USA) [35]. To ensure measurement accuracy, each nanofluid sample was tested three times, and the results were averaged.

Test for dynamic viscosity of GNP nanofluid

The viscosity of a fluid is a fundamental property that characterizes its resistance to flow under shear. The dynamic viscosity of the nanofluid was carried out using an NDJ-8S rotary viscometer with rotor 1 (spindle LV-1 61) at 6, 12, 30, and 60 rpm and temperatures from 30°C to 80°C.

Table 2. Weight composition of nanofluid concentrations.

Sample name	Aquades (g)	GNP (g)	Surfactant	
			Type	Mass (g)
0.1 wt%-NS	250	0.25	—	—
0.3 wt%-NS	250	0.75	—	—
0.6 wt%-NS	250	1.5	—	—
0.1 wt%-SDS	250	0.25	SDS	0.10
0.3 wt%-SDS	250	0.75	SDS	0.30
0.6 wt%-SDS	250	1.5	SDS	0.60
0.1 wt%-PVP	250	0.25	PVP	0.10
0.3 wt%-PVP	250	0.75	PVP	0.30
0.6 wt%-PVP	250	1.5	PVP	0.60

Test for stability of GNP nanofluid

The stability of GNP in the nanofluid was evaluated using both visual and quantitative methods based on sedimentation levels to assess the homogeneity of GNP dispersion over time. In the visual method, nanofluid samples were placed in transparent test tubes and kept at room temperature for 30 days [36]. Observations were conducted every 5 days to monitor any sedimentation or color changes. For the quantitative method, the sedimentation ratio (SR%) was calculated by measuring the height of the sediment (H) relative to the total height of the 1nanofluid in the tube (H_o), providing a numerical indication of sediment stability. The sedimentation, is examined using Equation (2) [37].

$$SR(\%) = \left(\frac{H}{Ho}\right) \times 100\% \quad (2)$$

SR% is used to assess the stability level of the nanofluid. If the SR value approaches 0%, it means that almost all particles have settled, indicating poor stability. If the SR value approaches 100%, it means the nanofluid remains stable without significant sedimentation [9].

Test for rheology of GNP nanofluid

The rheological behavior of GNP-based nanofluids to understand their flow characteristics under different concentrations and surfactant conditions. To provide deeper insight into the flow behavior, rheological analysis was carried out using the power law model, which is widely applied to describe non-Newtonian fluids. The relationship between shear stress (τ) and shear rate ($\dot{\gamma}$) as described by Equation (3) and shown in Fig. 3, where variations in shear rate (γ) were applied to evaluate the changes in viscosity relative to shear stress [38].

$$\tau = K \cdot \dot{\gamma}^n \quad (3)$$

Which is suitable for the Couette configuration of the viscometer used, where ω is the angular velocity (rad/s), is the container radius, and R_b is the spindle radius, as illustrated in Fig. 2 [39].

The shear rate ($\dot{\gamma}$) was determined based on the Couette geometry of the viscometer using Equation (4) [25].

$$\dot{\gamma} = \frac{2\omega R_c^2 R_b^2}{R_b^2(R_c^2 - R_b^2)} \quad (4)$$

Once shear rate was obtained, shear stress (τ) can be calculated using Equation (5), where η is the dynamic viscosity [25, 38].

$$\tau = \eta \cdot \dot{\gamma} \quad (5)$$

To determine the flow behavior index (n) and consistency index (K), the values of log(τ) were plotted against log ($\dot{\gamma}$). The slope of the resulting linear curve corresponds to n, and the intercept gives the value of K [40]. This analysis is performed to classify the nanofluid as either Newtonian or non-Newtonian fluid based on the viscosity characteristics relative to shear rate, as conducted in this study. This combined approach enables classification of the nanofluid as Newtonian ($n \approx 1$) or non-Newtonian ($n \neq 1$), while also explaining how surfactant type and GNP concentration affect viscosity behavior under applied shear [41].

Computational fluid dynamic modeling and simulation for thermal efficiency

Geometric dimension of heat exchanger

The CFD analysis in this study was conducted using computer-aided design with Ansys Fluent 2024 R1 software. The heat exchanger design adopts research by Behera *et al.* [42] and is simulated using the same boundary condition parameters. The heat exchanger design includes the addition of five baffles to modify the flow, allowing the fluid to have a longer residence time and to induce turbulence within the shell. The shell section uses aluminum material, and the tube uses copper material. To ensure realistic thermal performance, the operating temperature range was set between 40°C and 85°C, reflecting actual working conditions [25]. In this study, a counter-flow configuration was exclusively applied within the shell and tube heat exchanger, where nanofluid flows through the shell side and nanofluid through the tube side. A tube and shell type heat exchanger has been designed and the requirements are described below in Table 3 and geometry 3D shown in Fig. 2.

Meshing

A fully mesh using poly-hexacore elements was applied to capture the complex geometry of the shell and tube heat exchanger (shown in Fig. 3a). Inflation layers were added near solid boundaries to resolve the boundary layer accurately. Mesh quality was ensured with skewness below 0.9 and orthogonal quality above 0.1, meeting CFD standards for numerical stability [42, 43]. The grid independence test was confirmed with a final mesh consisting of 3 488 117 cells, where no significant changes were observed in the heat transfer rate, ensuring the stability of numerical results [43]. Mesh quality validation was performed not only through skewness and orthogonality metrics, but also via near-wall resolution assessment using the non-dimensional wall distance (Y^+). The Y^+ distribution ranged from 1.7 to 29.7, with most wall regions falling within the transitional range ($5 < Y^+ < 30$), approaching the lower boundary of the log-law region consistent with the k-ω shear stress transport turbulence model [44]. Figure 3b illustrates the Y^+ distribution on the shell surface, demonstrating representative coverage of fluid-wall interactions. This configuration ensures that the simulation domain accurately captures velocity and temperature gradients while maintaining computational efficiency.

Boundary condition

The boundary conditions in the simulation were defined to accurately represent the experimental setup and ensure a realistic heat transfer process, as described below in Fig. 3c and Table 4. All heat exchanger wall surfaces were assigned a no-slip condition.

The fluid domain was modeled using the experimentally tested nanofluids with various surfactant types, whose thermophysical properties (density, viscosity, thermal conductivity, and specific heat) are provided in Table 9. For the solid domain, materials were assigned as copper and aluminum based on the component

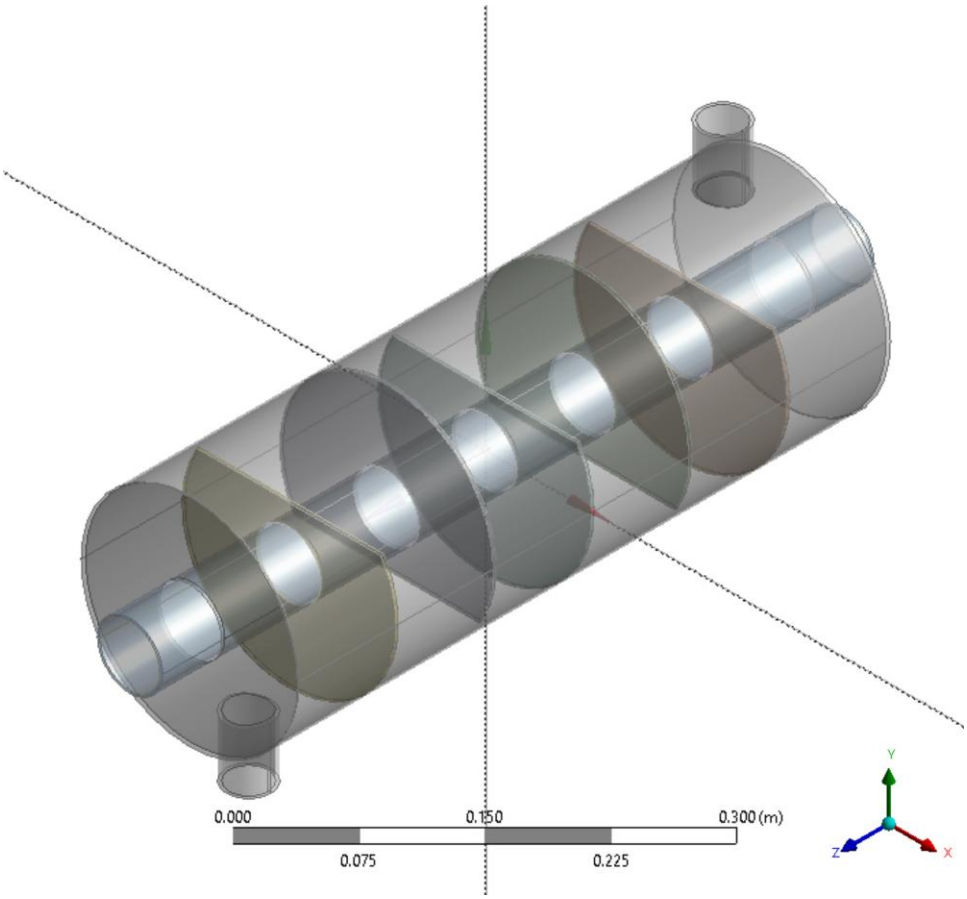

Figure 2. Geometry 3 dimension shell and tube heat exchanger.

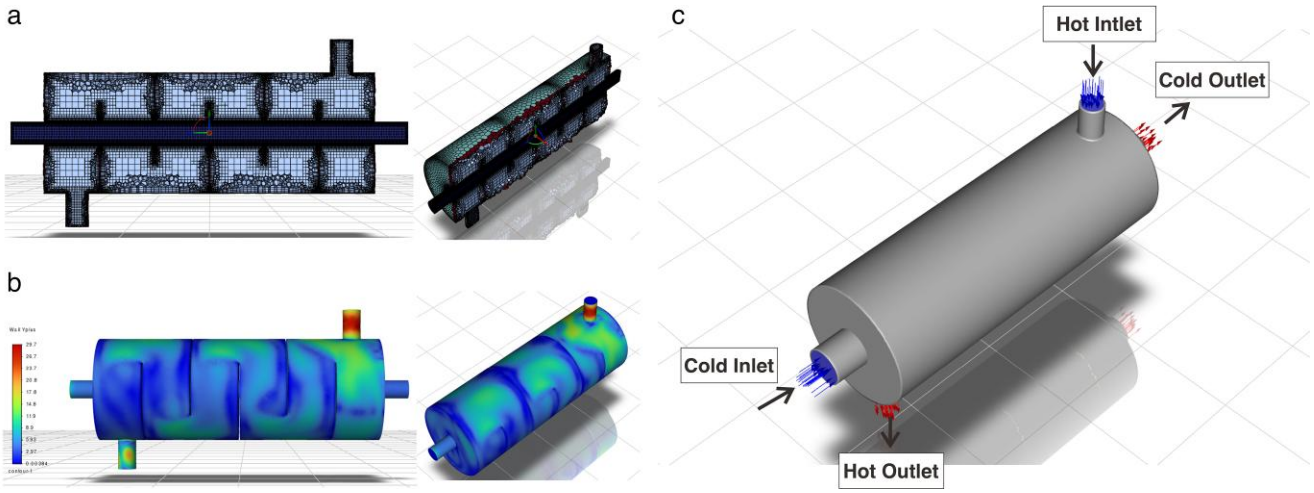

Figure 3. (a) The mesh using poly-hexacore elements, (b) validation of mesh quality based on wall Y^+ distribution, and (c) movement of hot and cold fluid.

structure and their respective thermal conductivities. Additionally, the energy equation was activated to accurately model the heat transfer process throughout the system.

Computational fluid dynamic solver configuration

During the solving stage, the simulation was carried out under steady-state conditions. The momentum equations for velocity and pressure were solved using the SIMPLE algorithm (semi-implicit method for pressure linked equations). The simulation used a Second Order Upwind scheme with residual criterion of 10^{-5} was set for all variables, the simulation steps run until residuals reached a steady state [42].

Result contour temperature set up

Temperature distribution was visualized using temperature contour plots sliced along an XY plane through the model [42]. This visual analysis helped evaluate heat transfer effectiveness and compare nanofluid performance. Temperature data at inlets

Table 3. Geometric dimension of heat exchanger [42].

Shell details	Dimensions
Outer diameter	182.5 mm
Inner diameter	180 mm
Length of the HE	500 mm
No. of baffles	5
Distance b/n baffles	80 mm
Tube details	**Dimensions**
Outer diameter	34.5 mm
Inner diameter	32 mm
No. of tubes	Single

Table 4. Boundary conditions taken into consideration.

Specification	Parameter	Value	Unit
Inlet	v_{in},c	1.5	m/s
	v_{in},h	0.5	m/s
	T_{in},c	20	°C
	T_{in},h	85	°C
Outlet	P_{out},c	0	Pa
	P_{out},h	0	Pa
Wall	$T_{Solid\ Shell}$	22	°C
	$T_{Solid\ Tube}$	22	°C

and outlets were extracted using surface integral tools with area-weighted average settings. These values formed the basis for calculating thermal effectiveness and were validated against experimental results [45].

Data processing for efficiency

Thermal efficiency calculations are performed to evaluate the heat transfer performance of the shell and tube heat exchanger simulation data obtained. Calculate cross-sectional area of the tube using Equation (6) [46], as follow:

$$A = \frac{\pi D^2}{4} \tag{6}$$

It is known that D is the inside diameter of the tube (m) and A is the cross-sectional area (m^2).

$$\dot{m} = \rho \,.\, A \,.\, V \tag{7}$$

Mass flow rate represents how much mass of fluid passes per second (Equation 7). It is a critical variable because heat transfer is proportional to the amount of mass moving through the system. This equation combines density (ρ) of the fluid (kg/m^3), A (m^2), V (flow velocity, m/s), and $\dot{m}$ (mass flow rate, kg/s) [47].

$$Q_{absorbed} = \dot{m}_c \times C_{p,c} \times (T_{out,cold} - T_{in,cold}) \tag{8}$$

The variable $\dot{m}_c$ represents the mass flow rate of the cold fluid in Equation (8), indicating how much mass passes through the system per unit time. $C_{p,cold}$ is the specific heat capacity of the cold fluid, measured in joules per kilogram per kelvin (J/kg·K), and it reflects the fluid's ability to store thermal energy. $T_{out,cold}$ and $T_{in,cold}$ denote the inlet and outlet temperatures of the cold fluid, respectively, showing the temperature before entering and after leaving the heat exchanger [48]. These parameters together are used to calculate the amount of heat absorbed by the cold fluid during the heat exchange process.

Table 5. Intensity, FWHM, d-spacing, and crystallite size of GNP.

Sample	XRD peak			
	Intensity (counts)	FWHM (rad)	d-spacing (Å)	Crystallite size (nm)
GNP	8198.17	0.2558	3.37189	100

$$Q_{released} = \dot{m}_h \times C_{p,hot} \times (T_{in,hot} - T_{out,hot}) \tag{9}$$

The term $Q_{released}$ represents the heat released by the hot fluid in the heat exchanger using Equation (9). It is calculated by multiplying the mass flow rate of the hot fluid, denoted as $\dot{m}_h$, by its specific heat capacity $C_{p,hot}$ (measured in joules per kilogram per kelvin, J/kg·K), and the temperature difference between the hot fluid's inlet temperature $T_{in,hot}$ and outlet temperature $T_{out,hot}$. These parameters quantify how much thermal energy the hot fluid loses as it flows through the heat exchanger [46].

$$\eta = \frac{Q_{absorbed}}{Q_{released}} \times 100\% \tag{10}$$

This is the final performance indicator of the heat exchanger is efficiency thermal using Equation (10). The result demonstrates the efficiency of heat transfer from the hot fluid stream to the cold stream in the system [25]. The calculation results of each parameter are then compared between nanofluid variations based on surfactant type (SDS, PVP, no surfactant) and concentration (0.1%, 0.3%, 0.6%) to determine the most optimal conditions in increasing thermal efficiency compared to conventional fluids (water).

Results and discussion

GNP characterization

Phase and crystallite size of GNP

The XRD analysis of the GNP was conducted to determine the phase composition and estimate the crystallite size [49]. The crystallite size was evaluated using the Scherrer equation [50], as presented in Equation (11).

$$d = \frac{k \times \lambda}{\beta \cos\theta} \tag{11}$$

The obtained calculated XRD results are summarized in Table 5 and shown in Fig. 4a.

Figure 4a illustrates the XRD pattern of GNP synthesized. The prominent and sharp diffraction peak observed at $2\theta = 26.43°$ corresponds to the (002) crystallographic plane of graphite, with a high intensity of 8198.17 counts, a d-spacing of 3.37 Å, and a narrow full width-half maximum of 0.2558 rad, indicating a well-ordered layered structure with high crystallinity. The calculated crystallite size using the Scherrer equation is approximately 100 nm [51]. In addition to the dominant at $2\theta = 42.36°$ and 54.53°, likely corresponding to (002) and (004) planes of graphite. These peaks may be attributed to interlayer stacking faults, oxygen-containing functional groups, or residual amorphous carbon phases, which are typical in graphene derived from biomaterials or via incomplete reduction [50, 52]. Notably, low-intensity peaks at higher angles (e.g. 77.41°–86.96°) indicate minor crystal irregularities or structural defects, which can influence electron

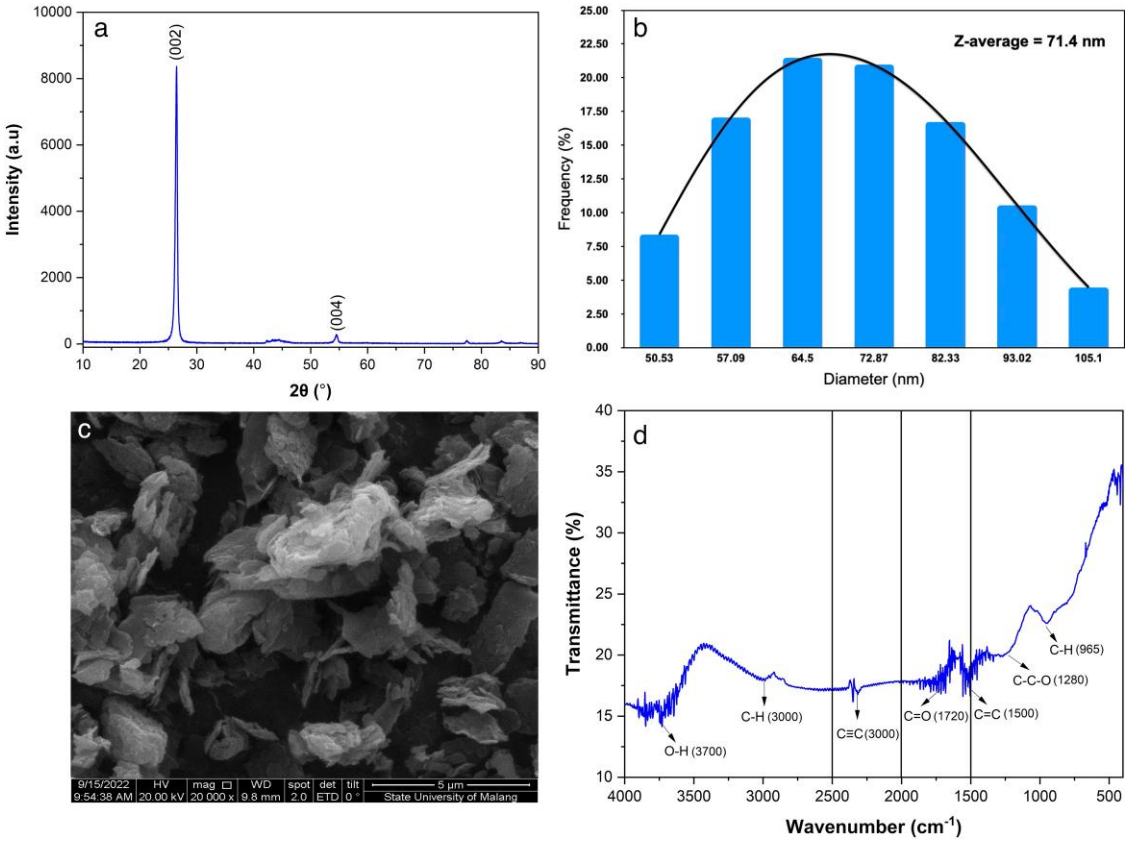

Figure 4. (a) XRD, (b) PSA, (c) SEM, and (d) FTIR results of GNP.

mobility and surface reactivity beneficial traits in nanofluid applications where interfacial phenomena dominate.

Particle size distribution of GNP

Figure 4b shows the PSA of the GNP with Z-average diameter is approximately 71.4 nm, with a size distribution ranging from 50.53 to 105.1 nm, reflecting the polydispersity commonly observed in top-down exfoliation or chemical synthesis processes. The majority of particles fall in the 65–85 nm range, supporting the crystallite size estimation from XRD, and confirming the presence of multilayer graphene sheets [53]. These sizes are included in the category of nanoparticles, namely those that have a size of less than 100 nm. One significant aspect of nanoparticle enhancement is attributed to Brownian motion, which plays a crucial role depending on the size and dispersion stability of the nanoparticles. Smaller nanoparticles are generally better at improving thermal conductivity due to their higher specific surface area, which provides more contact points for thermal energy transfer [34, 47]. However, there are discussions in the literature suggesting that while Brownian motion contributes to enhanced thermal performance, it is not the sole mechanism; rather, the resultant interactions between the base fluid's molecules can also foster localized heat transfer improvements [54].

Morphology of GNP

SEM analysis was carried out to identify the morphology of the GNP. The SEM form Fig. 4c illustrates that the particle morphology of the GNP the flat (planar) graphene particle structure stacked on top of each other, forming thin layers, which is characteristic of nanoplatelet morphology [55]. The particle surfaces appear as sheets that peel or layer, reinforcing the statement that graphene particles have a high surface area-to-volume ratio [56]. This leads to van der Waals forces between layers attracting each other to reduce surface energy, resulting in a thermodynamically more stable structure [57].This stacking structure supports the conclusion that graphene morphology significantly influences the enhancement of the nanofluids thermal conductivity by providing efficient pathways for heat transfer. Although the platelet structure improves thermal conductivity, previous studies have shown that its conductivity is still lower compared to cylindrical or brick-like structures [32]. The order of thermal conductivity from lowest to highest is platelets ≈ blades < bricks < cylinder.

Functional groups of GNP

The FTIR characterization was conducted to find the functional group of GNP. The results of FTIR are illustrated in Fig. 4d and Table 6.

Figure 4d presents the FTIR spectrum of GNP, revealing several key functional groups on the particle surface [60]. The broad peak observed at 3700 cm^{-1} corresponds to the O–H stretching vibration, indicating the presence of hydroxyl groups, which may result from surface oxidation [58]. The peaks near 3000 cm^{-1}, including those at 2904.80 cm^{-1}, 2947.23 cm^{-1}, and 3084.18 cm^{-1}, are attributed to C–H stretching vibrations, suggesting the existence of aliphatic or aromatic hydrocarbon chains [59]. A distinct band at 2305 cm^{-1} is associated with C≡C triple bond stretching, which is uncommon but can appear in functionalized graphene [59]. The peak at 1720 cm^{-1} signifies the presence of C=O stretching, indicating carbonyl groups such as carboxylic acid or ketone [60]. Additionally, the signal at 1500 cm^{-1} corresponds to C=C

Table 6. Functional groups of GNP.

Band	Main peak	Wave number	Typical bond assignment	Reference
1	3700	3700–3584	O–H stretching alcohol	Bello *et al.*, [58]
2	3000	3000–2800	C–H stretching alkene	Pang *et al.*, [59]
3	2305	2325–2290	C≡C disubstituted alkynes	Pang *et al.*, [59]
4	1720	1720	C = O carboxyl stretching	Kartick *et al.*, [60]
5	1500	1500–1450	C = C aromatic rings	Tran *et al.*, [61]
6	1280	1310–1250	C–C–O aromatic esters	Kartick *et al.*, [60]
7	965	965	C–H vinyl *trans*-disubstituted alkenes	Bello *et al.* [58]

stretching vibrations, characteristic of the aromatic structure of graphene's sp^2 carbon network [61]. The band at 1280 cm^{-1} is linked to C–C–O stretching vibrations, which can be assigned to epoxy or ether groups [60]. Lastly, the peak at 965 cm^{-1} indicates C–H out-of-plane bending, further confirming the presence of aromatic structures [58]. These functional groups suggest partial oxidation and confirm that the GNP possess a chemically stable structure dominated by single bonds. Table 9 shows that the GNP are classified as a single-bond group. A single bond is formed when a pair of electrons is divided into two atoms. This bond is relatively frail with smaller electron density than the double and triple bonds, but it has the most excellent stability due to its lower reactivity which results in more minimum electron loss [62]. Besides, the platelet morphology in the graphene also reflects its stability toward electron beam radiation.

Properties of GNP nanofluid

Density of GNP nanofluid

Based on Fig. 5 and Table 7, density increases with both GNP concentration and surfactant type, where the highest value (1007.91 ± 0.03 kg/m³) was recorded in the 0.6 wt% SDS-based sample. This trend is attributed to the high intrinsic density of GNP and the enhanced dispersion stability provided by SDS molecules, which reduce agglomeration and allow for more uniform particle suspension. Nanofluid density significantly influences heat transfer performance by affecting Reynolds number (Re), pressure drop, and thermal energy storage capacity [63]. Mechanistically, the addition of GNP increases the total mass per unit volume, thereby improving the nanofluids specific heat capacity and thermal inertia. This enhances the fluid's ability to store and transfer thermal energy efficiently [63, 64]. However, higher density also increases viscous resistance, which can impact pumping requirements [6, 65]. Hence, the balance between thermal benefits and hydrodynamic penalties must be considered in PVT heat exchanger applications. These findings not only confirm experimental trends but also offer a physical explanation grounded in nanofluid thermophysics, providing a strong basis for CFD simulation and system optimization.

Viscosity of GNP nanofluid

The viscosity of nanofluids is a critical parameter affecting heat transfer and thermal efficiency in heat exchangers within PVT systems. Based on the data shown in Fig. 6 and Table 7 indicate that nanofluid viscosity tends to increase with rising nanoparticle concentration, as seen in the non-surfactant (NS) samples and those with SDS surfactant, reaching average values up to 0.00299 Pa·s at 0.6 wt%-NS and 0.00219 Pa·s at 0.6 wt%-SDS. In contrast, samples with PVP surfactant maintain lower and relatively stable viscosity values, ranging from 0.00150 to 0.00195 Pa·s across the concentration range. Additionally, increasing temperature has a significant effect in reducing viscosity, for example at 80°C, viscosity can drop as low as 0.0015 Pa·s in the 0.1 wt%-PVP sample. These viscosity variations strongly influence heat transfer mechanisms, as optimal viscosity can enhance convection and improve heat transfer coefficients. Research by Emmanuel *et al.* [66] indicates that nanofluids with controlled viscosity can significantly enhance heat transfer efficiency in PVT systems by maximizing thermal contact and maintaining stable heat flow. Furthermore, Kadhum and Abed [67] emphasize that surfactants not only improve nanofluid stability but also play a role in optimizing viscosity, thereby improving heat exchanger thermal efficiency without compromising fluid flow. The PVP-based nanofluids are attributed to steric stabilization mechanisms, where PVP chains form a physical barrier around nanoparticles, preventing van der Waals-induced agglomeration. SDS, on the other hand, provides electrostatic stabilization through repulsion among similarly charged particles, although its effectiveness varies with concentration and ionic strength.

Thermal conductivity of GNP nanofluid

Thermal conductivity is a critical thermophysical property that governs the heat transfer behavior of nanofluids, particularly in PVT heat exchanger applications. As shown in Fig. 7 and Table 7, the highest thermal conductivity value was observed for the 0.3 wt% GNP-PVP sample, reaching 0.696 W/m·K, followed by the 0.1 wt%-PVP and 0.6 wt%-SDS samples. Mechanistically, thermal conductivity in nanofluids is influenced by several interrelated factors, including particle shape, volume fraction, Brownian motion, interfacial thermal resistance, and surfactant nanoparticle interactions [16]. This behavior aligns with the understanding that nanofluids have an optimal concentration range where the balance between nanoparticle dispersion and fluid dynamics results in maximum thermal conductivity [16].

The performance differences among surfactants also underline the importance of their molecular mechanisms: SDS offers electrostatic stabilization but is more sensitive to ionic strength, while PVP provides more robust steric stability across concentrations, preventing agglomeration and enhancing phonon transport [16]. However, at higher concentrations at 0.6 wt%-PVP, thermal conductivity decreased, likely due to particle clustering, increased viscosity, and disrupted thermal continuity, which hinder effective heat transfer [22]. The non-linear trend highlights the critical role of surfactant-nanoparticle interactions in forming effective thermal conduction networks. Moreover, particle morphology such as platelets, as in this study, contributes moderately to conductivity improvement due to limited interfacial contact compared to cylindrical structures [68]. These results indicate that optimizing thermal conductivity alone is insufficient for enhancing nanofluid performance. It must be evaluated alongside viscosity, specific heat, and stability to achieve maximum efficiency. In the context of PVT systems, thermal performance is maximized when all thermophysical properties are tuned synergistically [22, 69].

Stability of GNP nanofluid

Stability testing showed that PVP at all concentrations, as well as the 0.6 wt%-SDS sample, exhibited the highest stability, with no sedimentation observed up to Day 30, as presented in Fig. 8 and the nanofluid sedimentation observation results shown in

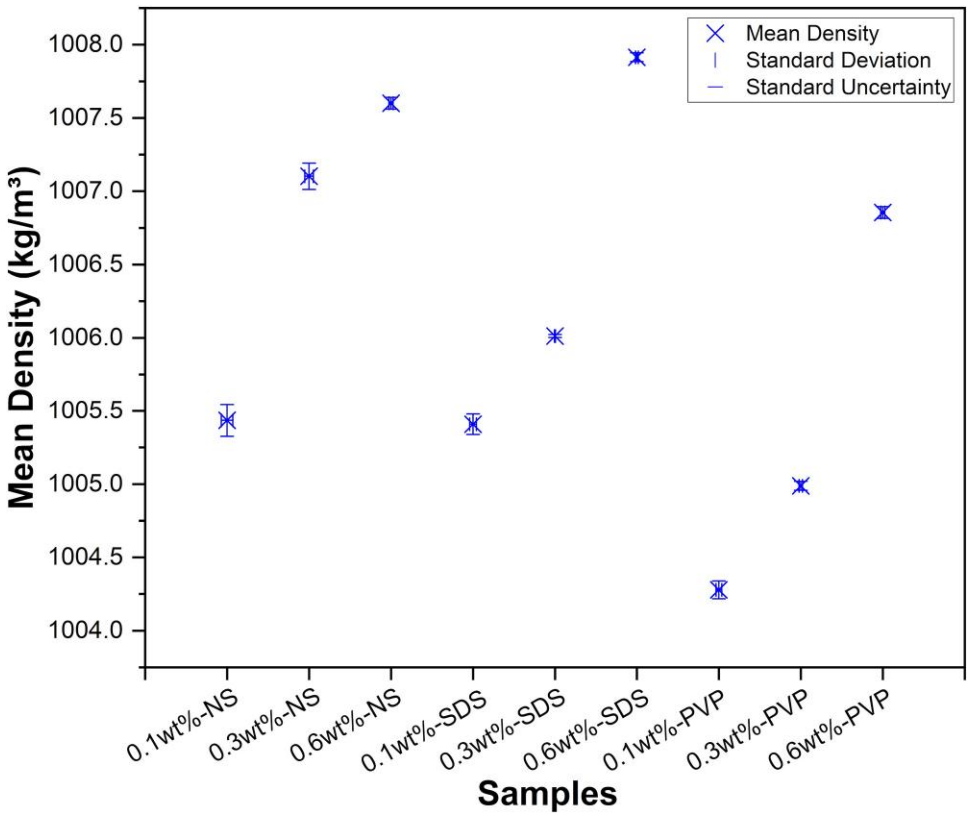

Figure 5. Results of GNP nanofluids density.

Table 7. Material properties of GNP nanofluids.

Sample	Mean density (kg/m³) ± SD	Std. unc.	Mean viscosity (Pa·s) ± SD	Std. unc.	Mean thermal conductivity (W/m·K)	Std. unc.	Specific heat (J/kg·K)
Water	997.000	—	0.00080 ± 0.000003	0.00376	0.310	—	4180.000
0.1 wt%-NS	1005.435 ± 0.11	0.0702	0.00192 ± 0.000003	0.00156	0.582 ± 0.024	0.014	4178.572
0.3 wt%-NS	1007.102 ± 0.09	0.0529	0.00188 ± 0.000003	0.00159	0.533 ± 0.028	0.016	4171.747
0.6 wt%-NS	1007.600 ± 0.04	0.0252	0.00299 ± 0.000004	0.00134	0.602 ± 0.021	0.012	4161.579
0.1 wt%-SDS	1005.408 ± 0.07	0.0410	0.00172 ± 0.000002	0.00117	0.595 ± 0.005	0.003	4176.984
0.3 wt%-SDS	1006.012 ± 0.01	0.0058	0.00208 ± 0.000002	0.00096	0.575 ± 0.018	0.010	4167.000
0.6 wt%-SDS	1007.914 ± 0.03	0.0173	0.00219 ± 0.000002	0.00091	0.632 ± 0.031	0.018	4152.116
0.1 wt%-PVP	1004.278 ± 0.06	0.0351	0.00150 ± 0.000003	0.00200	0.633 ± 0.021	0.012	4177.387
0.3 wt%-PVP	1004.988 ± 0.03	0.0208	0.00192 ± 0.000004	0.00208	0.696 ± 0.056	0.032	4168.201
0.6 wt%-PVP	1006.855 ± 0.04	0.0252	0.00195 ± 0.000002	0.00102	0.553 ± 0.007	0.004	4154.518

Supplementary File 1. The PVP is effective in forming a steric barrier that prevents nanoparticle agglomeration [68]. In contrast, nanofluids without surfactants experienced a significant decline in stability, with the highest sedimentation recorded in the 0.6 wt%-non-surfactant sample (0.2615% on day 30). The use of SDS improved stability but was only optimal at the 0.6 wt% concentration, while lower concentrations still exhibited slight sedimentation. Nanofluid stability is essential for maintaining thermal performance because particle sedimentation can reduce heat transfer effectiveness [5]. When nanoparticles settle, particle distribution within the fluid becomes uneven, leading to decreased thermal conductivity and the formation of stagnant zones in the heat exchanger [24]. This not only lowers the efficiency of heat absorption and release but can also disrupt flow rate. Therefore, high stability is crucial to ensure that the nanofluid remains homogeneous and effective in conducting heat throughout the operation of the PV/T system. Hence, a nanofluid with long-term colloidal stability not only sustains optimal thermal performance but also minimizes maintenance requirements, reduces the risk of clogging, and prolongs the operational lifespan of the PVT heat exchanger system. This makes PVP-based GNP nanofluids a more viable and sustainable choice for real-world solar thermal applications.

Rheology of GNP nanofluid

The rheological evaluation revealed that all synthesized nanofluids exhibited non-Newtonian, shear-thinning (pseudoplastic) behavior, characterized by flow behavior index (n) values below 1 as shown in Table 8. Among all samples, the 0.6 wt% nanofluid

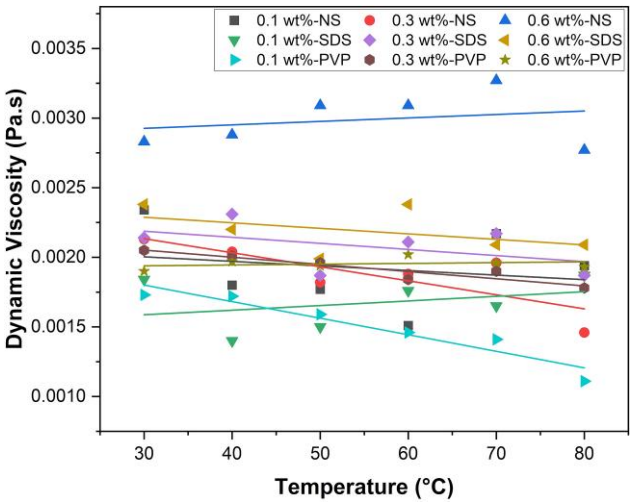

Figure 6. Results of GNP nanofluids viscosity with temperature variation.

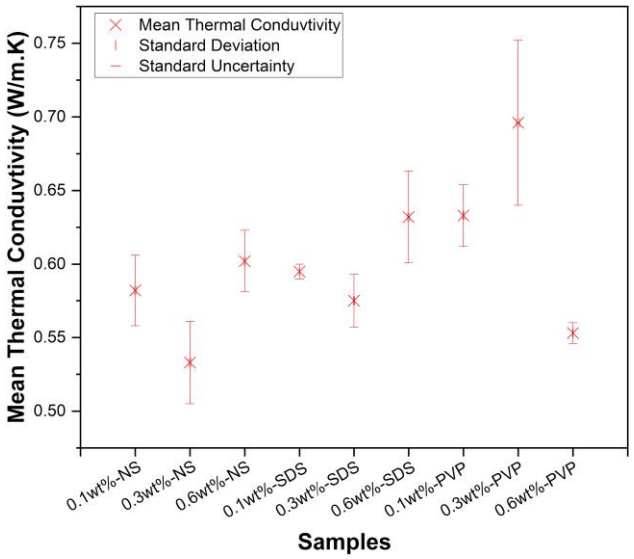

Figure 7. Results of thermal conductivity of nanofluids at various GNP concentrations and surfactant types. Error bars represent standard deviation ($n = 3$).

without surfactant (NS) consistently demonstrated the lowest n and highest consistency index (K) values as shown in Table 9, indicating stronger viscosity and more pronounced shear-thinning response. This implies that at low shear regions (e.g. laminar zones), the fluid resists flow, while at high shear regions (e.g. near heated surfaces), viscosity decreases, allowing enhanced convective heat transfer. However, excessive viscosity can also lead to higher pumping power requirements and a greater risk of sedimentation, which is detrimental for long-term PVT operation [69].

The addition of surfactants, particularly PVP, significantly modified the flow behavior by increasing n and reducing K. For instance, the 0.1 wt%-PVP sample displayed nearly Newtonian behavior at elevated temperatures ($n \approx 0.793$ at 80°C) with the lowest K values, indicating low resistance to flow and excellent stability, owing to the steric hindrance provided by PVP chains around the nanoplatelets. This contributes to better fluid circulation, reduces flow resistance, and minimizes agglomeration, making it a promising candidate for thermal applications [69].

In contrast, SDS-based nanofluids showed moderate shear-thinning with intermediate n and K values. The electrostatic stabilization offered by SDS is susceptible to ionic strength and concentration variations, leading to less consistent rheological behavior compared to PVP. Moreover, increasing GNP concentration generally lowered n and increased K across all surfactants, supporting the notion that higher particle loading intensifies particle-particle interactions, increases fluid resistance, and amplifies shear-thinning effects [70]. On the other hand, the addition of surfactants especially PVP significantly increases the n value and lowers the K value, resulting in a more stable, easily flowing, and homogeneous fluid. The 0.1 wt%-PVP sample consistently demonstrates an ideal combination: an n value approaching 1 at higher temperatures, indicating nearly Newtonian flow, and a low K value, reflecting lower viscosity at low shear rates. This supports better circulation efficiency, reduces pump load, and enhances stability and lifespan of the fluid within the system.

Mechanistically, nanofluid rheology is governed by multiple interacting parameters, including particle concentration, interparticle forces, surfactant-polymer dynamics, temperature effects, and fluid microstructure evolution under shear stress. While this may theoretically enhance heat transfer, it also brings technical challenges, including higher pumping demands and potential clogging risks [71]. These effects influence not only viscosity

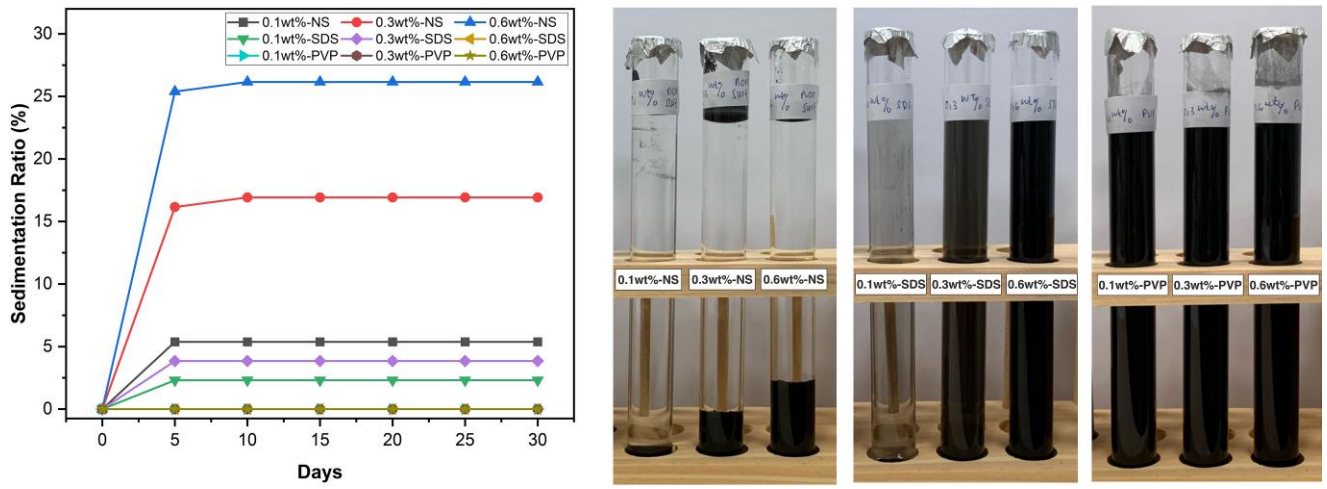

Figure 8. Sedimentation ratio of GNP nanofluids.

Table 8. Results of rheological testing for *n* (flow behavior index) values.

Samples	N					
	30°C	40°C	50°C	60°C	70°C	80°C
0.1 wt%-NS	0.250	0.431	0.462	0.583	0.239	0.302
0.3 wt%-NS	0.299	0.297	0.341	0.309	0.293	0.533
0.6 wt%-NS	0.291	0.266	0.190	0.187	0.158	0.266
0.1 wt%-SDS	0.458	0.702	0.503	0.441	0.486	0.422
0.3 wt%-SDS	0.341	0.310	0.353	0.365	0.297	0.347
0.6 wt%-SDS	0.382	0.347	0.342	0.318	0.341	0.346
0.1 wt%-PVP	0.461	0.488	0.482	0.606	0.613	0.793
0.3 wt%-PVP	0.341	0.310	0.353	0.365	0.297	0.347
0.6 wt%-PVP	0.382	0.347	0.342	0.318	0.341	0.346

Table 9. Results of rheological testing of consistency index (*K*).

Samples	*K* (Pa·s^n)					
	30°C	40°C	50°C	60°C	70°C	80°C
0.1 wt%-NS	0.0188	0.0088	0.0077	0.0050	0.0172	0.0135
0.3 wt%-NS	0.0149	0.0144	0.0116	0.0128	0.0139	0.0056
0.6 wt%-NS	0.0199	0.0218	0.0280	0.0280	0.0324	0.0207
0.1 wt%-SDS	0.0085	0.0034	0.0062	0.0085	0.0071	0.0095
0.3 wt%-SDS	0.0179	0.0206	0.0104	0.0149	0.0189	0.0107
0.6 wt%-SDS	0.0109	0.0124	0.0124	0.0137	0.0125	0.0122
0.1 wt%-PVP	0.0080	0.0074	0.0069	0.0046	0.0043	0.0021
0.3 wt%-PVP	0.0130	0.0138	0.0121	0.0111	0.0136	0.0112
0.6 wt%-PVP	0.0109	0.0124	0.0124	0.0137	0.0125	0.0122

but also flow stratification, turbulence generation, and heat transfer efficiency within heat exchangers. The optimal rheological balance was achieved at 0.1 wt%-PVP, which combines favorable flow behavior, system stability, and low energy cost. This is further validated by CFD results as shown in Fig. 9, confirming superior thermal efficiency over base fluid under simulated operating conditions.

Computational fluid dynamic simulation of heat exchanger in PVT system

Temperature contour of GNP nanofluids

Table 10 presents the results of outlet temperature values obtained from CFD simulations for various nanofluid samples with different surfactants and concentrations. In each case, the cold and hot fluid inlet temperatures were set at 20°C and 85°C, respectively. The simulated outlet temperatures both for the cold and hot sides demonstrate the thermal exchange performance of each sample. Table 10 provides a comparative summary of the inlet and outlet temperatures for both hot and cold fluids. The largest temperature gain on the cold side ($\Delta Tc = 0.775$°C) and the greatest heat release on the hot side ($\Delta Th = 5.192$°C) were achieved with the 0.3 wt% GNP + PVP sample, confirming superior heat absorption and extraction performance. These values surpass those of the base fluid ($\Delta Tc = 0.387$°C; $\Delta Th = 2.888$°C), illustrating a substantial enhancement in thermal exchange.

Notably, nanofluids with PVP exhibited higher outlet cold temperatures, suggesting effective heat pickup from the hot side, while the corresponding hot outlet temperatures dropped more sharply evidence of efficient thermal dissipation. In comparison, the 0.6 wt% NS sample, despite a marginally higher ΔTc than base water, showed reduced performance due to the influence of sedimentation and inconsistent flow, as inferred from the experimental data. Taken together, the integration of experimental thermophysical and stability data with the CFD simulation results provides a coherent explanation of how nanofluid formulation impacts thermal behavior. The enhanced ΔT values, combined with supportive visual evidence from temperature contours, validate the practical potential of surfactant-modified GNP nanofluids particularly with PVP at 0.3 wt% in improving the thermal efficiency of PVT heat exchangers.

The CFD contour temperature plots support these numerical results shown in Fig. 10 and File S2, visually highlighting temperature gradients and heat distribution across the heat exchanger. The CFD temperature contour distribution reveals that the use

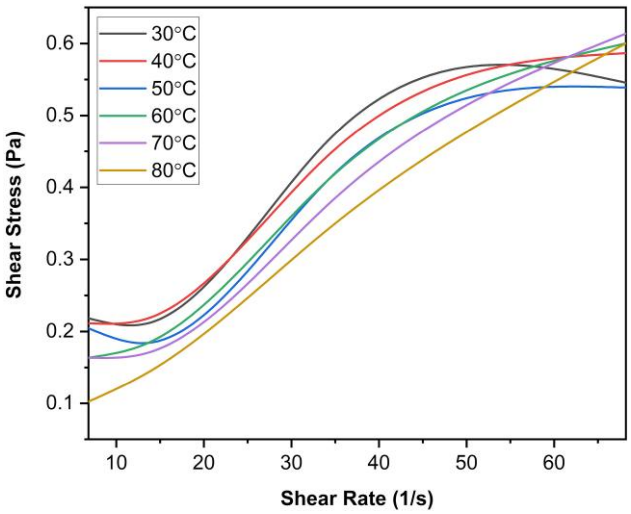

Figure 9. Rheology graph of 0.1 wt% GNP + PVP Sample.

of nanofluids significantly alters heat transfer patterns within the heat exchanger compared to the base fluid (water-to-water). The 0.3 wt% GNP + PVP sample exhibited the broadest and most uniform temperature gradient, indicating enhanced thermal exchange between hot and cold fluids. This finding is consistent with the experimental stability results, which showed that PVP-based nanofluids had the highest dispersion stability with no sedimentation up to Day 30. In addition, this sample demonstrated moderate viscosity with shear-thinning behavior and the highest thermal conductivity during thermophysical testing, which collectively contribute to effective convective heat transfer.

In contrast, nanofluids without surfactants or those using SDS at lower concentrations displayed limited contour distributions and uneven gradients, indicating possible stagnant zones due to nanoparticle sedimentation. This is in line with the poor stability observed in the sedimentation tests, and the lower thermal conductivity recorded during material characterization. The presence of these stagnant zones hinders thermal homogeneity and lowers heat transfer efficiency. Mechanistically, PVP forms a steric stabilization layer around the nanoparticles, preventing agglomeration during circulation. Although the addition of PVP increases fluid viscosity, its benefits in terms of dispersion stability and thermal conductivity outweigh the potential drawbacks of increased resistance to flow. These observations are supported by previous studies such as Karagiannakis *et al.* [16] and Al-Waeli *et al.* [6]

Table 10. Outlet temperature from CFD simulation.

Sample	$T_{in}c$ (°C)	$T_{in}h$ (°C)	$T_{out}c$ (°C)	$T_{out}h$ (°C)	ΔTc (°C)	ΔTh (°C)	$Q_{absorbed}$ (W)	$Q_{released}$ (W)
Water to Water	20	85	20.387	82.112	0.387	2.888	1945.266	4837.358
0.1 wt%-NS	20	85	20.652	80.648	0.652	4.352	3202.642	7351.211
0.3 wt%-NS	20	85	20.687	80.392	0.687	4.608	3485.139	7797.171
0.6 wt%-NS	20	85	20.692	80.359	0.692	4.641	3516.617	7856.407
0.1 wt%-SDS	20	85	20.637	80.745	0.637	4.255	3215.527	7186.382
0.3 wt%-SDS	20	85	20.648	80.669	0.648	4.331	3277.709	7319.881
0.6 wt%-SDS	20	85	20.740	80.038	0.740	4.962	3759.091	8402.433
0.1 wt%-PVP	20	85	20.732	80.150	0.732	4.850	3703.982	8182.985
0.3 wt%-PVP	20	85	20.775	79.808	0.775	5.192	3929.930	8749.771
0.6 wt%-PVP	20	85	20.682	80.427	0.682	4.573	3467.522	7735.325

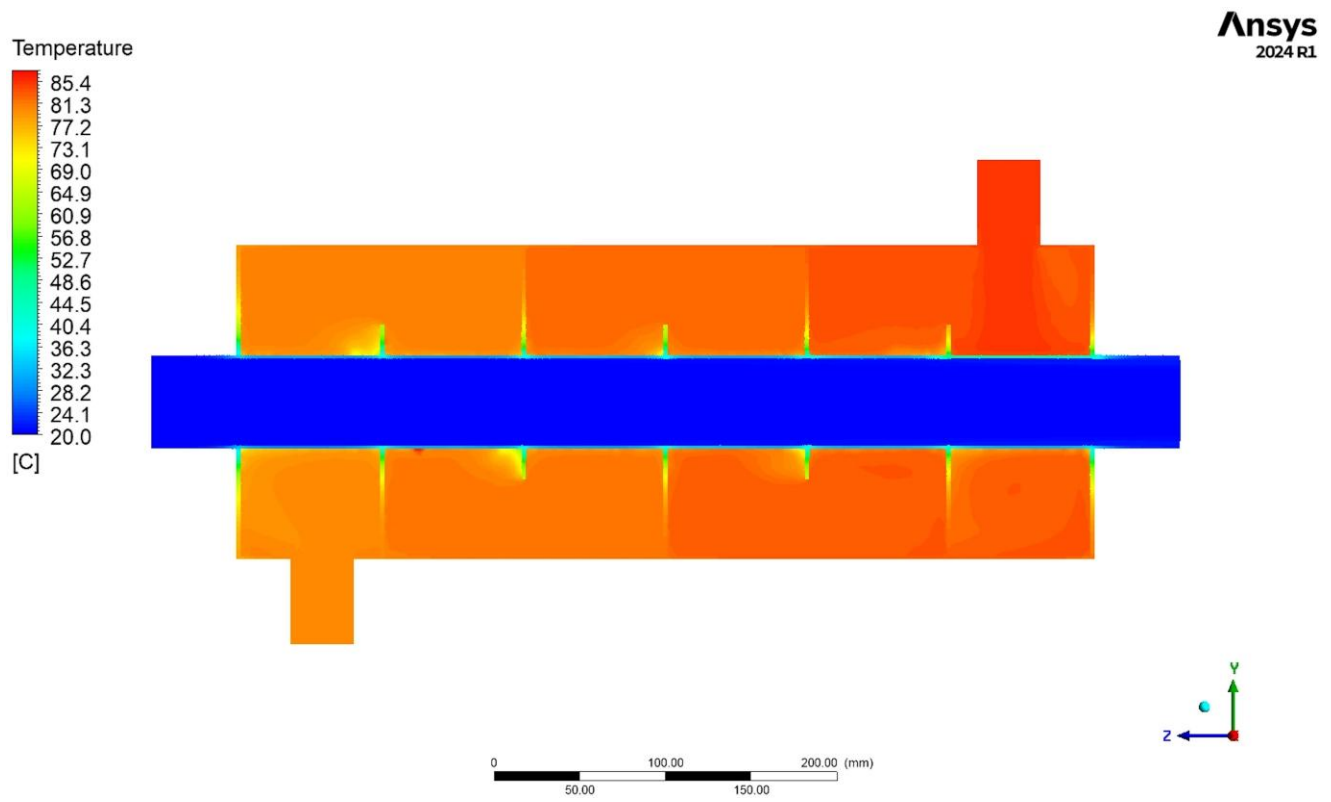

Figure 10. Temperature contour results for 0.1 wt%-PVP Sample from CFD simulation.

which emphasize the dominant role of dispersion stability over viscosity in determining nanofluid heat transfer effectiveness.

Thermal efficiency results from the use of GNP nanofluids

The thermal efficiency results presented in Fig. 11 show that using GNP-based nanofluids significantly enhances heat transfer performance compared to the base fluid (water-to-water), which achieved only 40.21% efficiency. Among all samples, the 0.1 wt% + PVP nanofluid had the highest thermal efficiency of 45.26%. This superior performance is attributed to its high thermal conductivity (0.633 W/m·K), specific heat capacity (4177 J/kg·K), low viscosity at high shear rate (0.0102 Pa·s), and favorable shear-thinning behavior ($n = 0.526$). The enhancement in thermal performance of PVT heat exchangers using GNP-based nanofluids is attributed to multiple interrelated mechanisms. First, the two-dimensional structure and high intrinsic thermal conductivity of GNP facilitate efficient phonon transport, significantly improving heat conduction within the fluid [72]. Second, the incorporation of the nonionic surfactant PVP improves colloidal stability by preventing nanoparticle agglomeration, resulting in more uniform dispersion and stable thermal behavior [73]. This combination promotes effective convection and uniform heat distribution in the heat exchanger [74].

Meanwhile, SDS-based samples also exhibited good and consistent thermal efficiencies, ranging between 44.74% and 44.78%, with the best result at 0.3 wt%-SDS. These samples showed moderate rheological properties ($n = 0.343$; $K = 0.0153$ Pa·s^n) and balanced viscosity, which helped

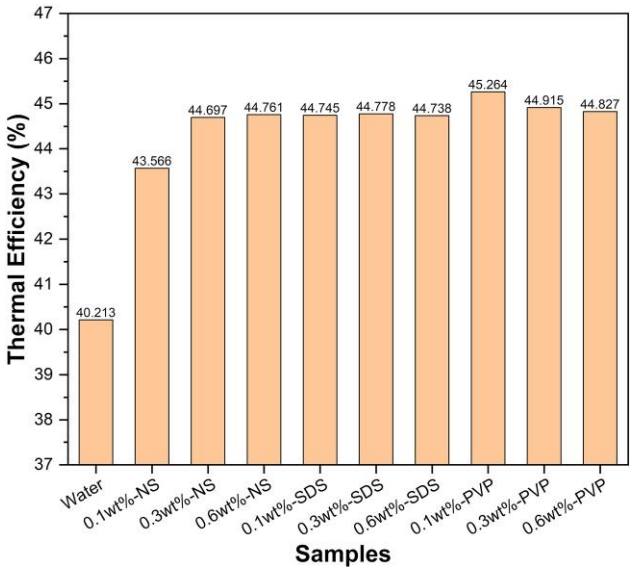

Figure 11. Results of thermal efficiency.

maintain flow without excessive pressure drops. However, the dispersion stability offered by SDS was not as strong as PVP, especially at lower concentrations, leading to partial sedimentation and potential long-term efficiency decline.

In contrast, NS nanofluids, despite having relatively good thermal conductivity (up to 0.602 W/m·K for 0.6 wt%), demonstrated lower and less consistent thermal efficiencies, ranging from 43.57% to 44.76%. This was primarily due to their higher viscosity (up to 0.0750 Pa·s) and highly non-Newtonian behavior (very low n, averaging 0.214–0.492), which hindered flow and caused the formation of stagnant zones in the heat exchanger. The absence of dispersing agents further led to nanoparticle agglomeration and sedimentation, as confirmed by the poor stability observed in the 30-day test.

This is primarily influenced by the increased viscosity of nanofluids, which can hinder fluid flow within the heat exchanger, thereby reducing convective heat transfer efficiency. The viscosity depends not only on nanoparticle concentration but also on the rheological properties of the nanofluid characterized by the flow behavior index (n) and consistency coefficient (K) from the Power Law model [69]. In CFD simulations, the values of n and K are incorporated to dynamically model viscosity changes according to real flow conditions, providing a more accurate representation of nanofluid performance. Nanofluids with $n<1$ (shear thinning) and moderate K tend to experience decreased viscosity at higher shear rates, which helps facilitate flow and improve thermal efficiency [75]. Overall, these findings confirm that thermal efficiency is not solely dependent on thermal conductivity, but also on dispersion stability, flow behavior (n and K), and dynamic viscosity characteristics [69]. The best-performing formulation was GNP + PVP at 0.1–0.3 wt%, which outperformed water and other nanofluids. By integrating detailed rheological and thermophysical properties into CFD simulations, this study provides more realistic and representative predictions of nanofluid performance under actual PVT operating conditions.

Given that the heat exchanger is a core component of PVT systems, its improvement directly enhances both thermal energy harvesting and PV panel cooling. Thus, optimizing the heat exchanger translates into a systemic boost in total energy output. For real-world applications, nanofluid formulations must balance thermal performance with long-term dispersion and hydrodynamic stability. Future research should involve field-scale validation and techno-economic assessments to ensure the scalability and viability of GNP-based nanofluids in solar energy systems, particularly in residential and light industrial settings.

Conclusions

This study investigated the effects of GNP nanofluids with various surfactants and concentrations on thermophysical properties, flow behavior, dispersion stability, and heat exchanger efficiency in PVT systems. Experimental measurements and CFD simulations confirmed that GNP nanofluids significantly enhance heat transfer performance compared to base fluid (water). The highest thermal efficiency was observed at 45.26% for the 0.1 wt% GNP + PVP nanofluid, compared to 40.21% for water a 12.6% relative improvement.

This enhancement is driven by a combination of superior thermal conductivity (0.633 W/m·K), high specific heat (4177 J/kg·K), low shear-dependent viscosity (0.0102 Pa·s), and favorable rheological behavior ($n=0.526$), all supported by strong dispersion stability (no sedimentation for 30 days). These findings align with previous literature but uniquely contribute by integrating rheological measurements into CFD simulations tailored to PVT system conditions. Compared to SDS and NS nanofluids, PVP-modified GNP nanofluids consistently demonstrated superior thermal efficiency and colloidal stability, confirming the critical role of surfactant type and concentration in optimizing nanofluid performance. Overall, this study validates the 0.1–0.3 wt% GNP-PVP formulation as the most effective and scalable nanofluid for solar thermal applications and proposes an integrated framework for evaluating nanofluid-enhanced heat exchangers in future renewable energy systems.

Acknowledgments

The authors would like to express their sincere gratitude to Muhammad Albin Abdiyar and Dharma Maheswara for their valuable support and insightful guidance in the Computational Fluid Dynamics (CFD) modeling and analysis conducted in this study. Figure 1 was created with BioRender under the author's Academic Publication License. Required attribution: "Created in BioRender. Pramono, D. (2025) https://BioRender.com/qsffzvk." The Completed Graphic is sublicensed with the article under CC BY 4.0; third-party reuse must provide proper attribution and comply with BioRender's License Terms when using or modifying BioRender assets.

Author contributions

Saiful Anwar (Data curation [equal], Formal analysis [equal], Visualization [equal], Writing—original draft [equal]), Poppy Puspitasari (Funding acquisition [lead], Resources [lead], Software [lead], Supervision [lead], Writing—review & editing [lead]), Diki Pramono (Conceptualization [lead], Formal analysis [equal], Investigation [equal], Methodology [lead], Writing—original draft [equal]), Avita Permanasari (Methodology [equal], Validation [equal], Writing—review & editing [equal]), Yahya Zakaria (Software [equal], Writing—review & editing [equal]), and Mohd Rosli (Validation [equal], Writing—review & editing [equal])

Supplementary data

Supplementary data is available at *Clean Energy* online.

Nomenclature

Symbol,	meaning;
v_{in},c,	inlet velocity of cold fluid (m/s);
v_{in},h,	inlet velocity of hot fluid (m/s);
P_{out},c,	outlet pressure of cold fluid (Pa);
P_{out},h,	outlet pressure of hot fluid (Pa);
$T_{Solid\ Shell}$,	temperature of solid shell (°C);
$T_{Solid\ Tube}$,	temperature of solid tube (°C);
$Q_{absorbed}$,	heat absorbed by the cold fluid (W);
$Q_{released}$,	heat released by the hot fluid (W);
$\dot{m}_c$,	mass flow rate of cold fluid (kg/s);
$\dot{m}_h$,	mass flow rate of hot fluid (kg/s);
C_p,c,	specific heat capacity of cold fluid (J/kg·K);
C_p,h,	specific heat capacity of hot fluid (J/kg·K);
T_{in},c,	inlet temperature of cold fluid (°C);
T_{out},c,	outlet temperature of cold fluid (°C);
T_{in},h,	inlet temperature of hot fluid (°C);
T_{out},h,	outlet temperature of hot fluid (°C);
ρ,	density (kg/m³);
η,	thermal efficiency (%);
n,	flow behavior index (dimensionless, from power law);
K,	consistency index (Pa·sⁿ, from Power Law);
μ,	dynamic viscosity (mPa·s);
$\dot{\gamma}$,	shear rate (s^{-1});
τ,	shear stress (Pa);
A,	cross-sectional area (m²);
D,	diameter of pipe (m);
SR,	sedimentation ratio (%)

.

Conflict of interest

None declared.

Funding

This work was supported by Universitas Negeri Malang for Kolaborasi Pendanaan Bersama/Matching Fund 2025 Research Grant (24.2.1213/UN32.14.1/LT/2025).

Data availability

Data available on request.

References

[1] Rozak AO, Mulyadi TR, Nurfadilah H. Analysis the effect of solar radiation on the efficiency of PV plant 50 kWp rooftop UNPAM viktor. *J Renew Energy Mech* 2023;**6**:63–76. https://doi.org/10.25299/rem.2023.vol6.no02.12181

[2] Shaik F, Lingala SS, Veeraboina P. Effect of various parameters on the performance of solar PV power plant: a review and the experimental study. *Sustain Energy Res* 2023;**10**:6. https://doi.org/10.1186/s40807-023-00076-x

[3] Jaya HS, Rahmat MH, Asrori A. Analisis Pengaruh Suhu Panel Surya Terhadap Output Panel Performance. *J Mech Eng* 2024;**1**:42–51. https://doi.org/10.47134/jme.v1i1.2189

[4] Rahman MA, Hasnain SMM, Pandey S *et al.* Review on nanofluids: preparation, properties, stability, and thermal performance augmentation in heat transfer applications. *ACS Omega* 2024;**9**:32328–49. https://doi.org/10.1021/acsomega.4c03279

[5] Moulefera I, Marín JJD, Cascales A *et al.* Innovative application of graphene nanoplatelet-based ionanofluids as heat transfer fluid in hybrid photovoltaic-thermal solar collectors. *Sci Rep* 2025;**15**:6489. https://doi.org/10.1038/s41598-025-91040-w

[6] Al-Waeli AHA, Chaichan MT, Kazem HA *et al.* Comparison study of indoor/outdoor experiments of a photovoltaic thermal PV/T system containing SiC nanofluid as a coolant. *Energy* 2018;**151**:33–44. https://doi.org/10.1016/j.energy.2018.03.040

[7] Kanti PK, Wanatasanappan VV, Said NM *et al.* Thermal performance, entropy generation, and machine learning insights of Al_2O_3-TiO_2 hybrid nanofluids in turbulent flow. *Sci Rep* 2025;**15**:16035. https://doi.org/10.1038/s41598-025-93749-0

[8] Baek S, Shin D, Kim G *et al.* Influence of amphoteric and anionic surfactants on stability, surface tension, and thermal conductivity of Al_2O_3/water nanofluids. *Case Stud Therm Eng* 2021;**25**:100995. https://doi.org/10.1016/j.csite.2021.100995

[9] Thakur P, Potoroko I, Sonawane SS. Stability of nanofluids. In: Sonawane SS, Sharifpur M (eds.) *Nanofluid Applications for Advanced Thermal Solutions*. Amsterdam: Elsevier Science, 2024, 43–62.

[10] Bahari NM, Hussein SNCM, Othman NH. Synthesis of Al_2O_3–SiO_2/water hybrid nanofluids and effects of surfactant toward dispersion and stability. *Part Sci Technol* 2021;**39**:844–58. https://doi.org/10.1080/02726351.2020.1838015

[11] Ali N. Graphene-based nanofluids: production parameter effects on thermophysical properties and dispersion stability. *Nanomaterials* 2022;**12**:357. https://doi.org/10.3390/nano12030357

[12] Kanti PK, Vicki Wanatasanappan V, Said NM *et al.* Stability, thermophysical properties, forced convective heat transfer, entropy minimization and exergy performance of a novel hybrid nanofluid: experimental study. *J Mol Liq* 2024;**410**:125571. https://doi.org/10.1016/j.molliq.2024.125571

[13] Kanti PK, Kumar PHG, Wanatasanappan VV *et al.* Graphene's Frontier in aerospace: current applications, challenges, and future directions for space engineering. *Nanoscale Adv* 2025;**7**:3603–18. https://doi.org/10.1039/D4NA00934G

[14] Sekhar YR, Chilambarasan L, Sharma KV *et al.* Solar flat plate collectors with internally grooved absorber tubes for enhanced efficiency: application of eXplainable artificial intelligence using cooperative game theory-based Shapley values. *Case Stud Therm Eng* 2025;**68**:105912. https://doi.org/10.1016/j.csite.2025.105912

[15] Sheikholeslami M, Alturaihi MH. Numerical analysis of thermal management in a photovoltaic Solar System with porous heat storage, parabolic reflector and self-cleaning coating. *Int Commun Heat Mass Transf* 2025;**164**:108847. https://doi.org/10.1016/j.icheatmasstransfer.2025.108847

[16] Karagiannakis NP, Skouras ED, Burganos VN. Modelling thermal conduction in nanoparticle aggregates in the presence of surfactants. *Nanomaterials* 2020;**10**:2288. https://doi.org/10.3390/nano10112288

[17] Kanti PK, Sharma P, Maiya MP *et al.* The stability and thermophysical properties of Al_2O_3-graphene oxide hybrid nanofluids for solar energy applications: application of robust autoregressive modern machine learning technique. *Sol Energy Mater Sol*

Cells 2023;**253**:112207. https://doi.org/10.1016/j.solmat.2023.112207

[18] Sheikholeslami M, Alinia AM. Energy management in a concentrated solar photovoltaic panel with a thermoelectric module and nanomaterial-filled storage tank. *Energy* 2025;**328**:136439. https://doi.org/10.1016/j.energy.2025.136439

[19] Kanti PK, Sharma P, Sharma KV *et al.* The effect of pH on stability and thermal performance of graphene oxide and copper oxide hybrid nanofluids for heat transfer applications: application of novel machine learning technique. *J Energy Chem* 2023;**82**:359–74. https://doi.org/10.1016/j.jechem.2023.04.001

[20] Mehrali M, Sadeghinezhad E, Akhiani AR *et al.* An ecofriendly graphene-based nanofluid for heat transfer applications. *J Clean Prod* 2016;**137**:555–66. https://doi.org/10.1016/j.jclepro.2016.07.136

[21] Safitri Y, Irwan I, Rahmawati CA. Pengaruh Penambahan Surfaktan Gum Arabic Terhadap Sifat Fisik dan Stabilitas Fluida Nano Titania (TiO_2). *J Teknol* 2021;**21**:26–31. https://doi.org/10.30811/teknologi.v21i1.2207

[22] Mirahmad A, Kumar RS, Doldán BP *et al.* Beyond thermal conductivity: a review of nanofluids for enhanced energy storage and heat transfer. *Nanomaterials* 2025;**15**:302. https://doi.org/10.3390/nano15040302

[23] Sheikholeslami M, Ali FAMA. Experimental evaluation of vortex generators for enhancing solar photovoltaic panel performance with parabolic reflectors. *Sol Energy Mater Sol Cells* 2025;**282**:113411. https://doi.org/10.1016/j.solmat.2025.113411

[24] Al-Waeli AHA, Chaichan MT, Kazem HA *et al.* Evaluation and analysis of nanofluid and surfactant impact on photovoltaic-thermal systems. *Case Stud Therm Eng* 2019;**13**:100392. https://doi.org/10.1016/j.csite.2019.100392

[25] Permanasari AA, Rosli MAM, Habibi IA *et al.* Efficiency of a photovoltaic thermal (PVT) system using bio-nanofluid based on virgin coconut oil-graphene with additive surfactant: an experimental study. *J Adv Res Appl Sci Eng Technol* 2023;**34**:287–304. https://doi.org/10.37934/araset.34.2.287304

[26] Rafaizul NIAM, Rosli MAM, Salimen N *et al.* Formulation of graphene nanoplatelets water-based nanofluids using polyvinylpyrrolidone (PVP) as surfactant. *J Adv Res Micro Nano Eng* 2024;**16**:35–47. https://doi.org/10.37934/armne.16.1.3547

[27] Abenante L, Penteado F, Vieira MM *et al.* Ultrasound-enhanced Ag-catalyzed decarboxylative coupling between α-keto acids and disulfides for the synthesis of thioesters. *Ultrason Sonochem* 2018;**49**:41–6. https://doi.org/10.1016/j.ultsonch.2018.07.014

[28] Feng BB, Wang ZH, Suo WH *et al.* Performance of graphene dispersion by using mixed surfactants. *Mater Res Express* 2020;**7**:095009. https://doi.org/10.1088/2053-1591/abb2ca

[29] Puspitasari P, Pramono DD, Fiansyah DN *et al.* Biodiesel production from waste cooking oil using calcium oxide derived from scallop shell waste. *Clean Energy* 2024;**8**:113–26. https://doi.org/10.1093/ce/zkae005

[30] Mori Y, Yoshida H, Masuda H. Particle size analysis by laser diffraction method using reference particles. *Adv Mater Res* 2012;**508**:33–7. https://doi.org/10.4028/www.scientific.net/AMR.508.33

[31] Schatten H, Pawley JB. *Biological Low-Voltage Scanning Electron Microscopy*. New York: Springer Science, 2008.

[32] Ebrahim SA, Pradeep E, Mukherjee S *et al.* Rheological behavior of dilute graphene-water nanofluids using various surfactants: an experimental evaluation. *J Mol Liq* 2023;**370**:120987. https://doi.org/10.1016/j.molliq.2022.120987

[33] Puspitasari P, Ayu Permanasari A, Ilman Hakimi Chua Abdullah M *et al.* Tribology characteristic of ball bearing SKF RB-12.7/G20W using SAE 5W-30 lubricant with carbon-based nanomaterial addition. *Tribol Ind* 2023;**45**:664–75. https://doi.org/10.24874/ti.1538.09.23.11

[34] Mariono M, Wahyudi W, Nadjib M. Effect of density and viscosity on injection characteristic of Jatropha—waste cooking oil biodiesel mixture. *JMPM* 2023;**7**:44–52. https://doi.org/10.18196/jmpm.v7i1.17896

[35] Selvam C, Mohan DL, Harish S. Thermal conductivity and specific heat capacity of water–ethylene glycol mixture-based nanofluids with graphene nanoplatelets. *J Therm Anal Calorim* 2017;**129**:947–55. https://doi.org/10.1007/s10973-017-6276-6

[36] Ma M, Zhai Y, Yao P *et al.* Effect of surfactant on the rheological behavior and thermophysical properties of hybrid nanofluids. *Powder Technol* 2021;**379**:373–83. https://doi.org/10.1016/j.powtec.2020.10.089

[37] Mukherjee S, Chakrabarty S, Mishra PC *et al.* Stability and sedimentation characteristics of water based Al_2O_3 and TiO_2 nanofluids. *Part N J Nanomater Nanoeng Nanosyst* 2024;**238**:17–30. https://doi.org/10.1177/23977914221127735

[38] Amin ATM, Hamzah WAW, Oumer AN. Thermal conductivity and dynamic viscosity of mono and hybrid organic- and synthetic-based nanofluids: a critical review. *Nanotechnol Rev* 2021;**10**:1624–61. https://doi.org/10.1515/ntrev-2021-0086

[39] Iqbal S, Naveed MF, Masud M *et al.* Experimental evaluation of thermal performance in shell and tube heat exchangers using $Al_2O_{3-\gamma}$ nanofluids†. *Eng Proc* 2024;**75**:13. https://doi.org/10.3390/engproc2024075013

[40] Ramli H, Zainal NFA, Hess M *et al.* Basic principle and good practices of rheology for polymers for teachers and beginners. *Chem Teach Int* 2022;**4**:307–26. https://doi.org/10.1515/cti-2022-0010

[41] Asim SB, Noviani E, Helmi H. Pemodelan Aliran Fluida Bidang Miring pada Lapisan Tipis. *J Mat Integr* 2023;**19**:125–36. https://doi.org/10.24198/jmi.v19.n1.40855.125-136

[42] Behera M, Nayak J, Bal S. Heat transfer analysis of CuO-ZnO/water hybrid nanofluid in a shell and tube heat exchanger with various tube shapes. *Int J Thermofluids* 2024;**24**:100972. https://doi.org/10.1016/j.ijft.2024.100972

[43] Kilic GA. Performance evaluation of triply periodic minimal surface heat exchangers using nanofluids at high flow rates for enhanced energy efficiency. *Appl Sci* 2025;**15**:4140. https://doi.org/10.3390/app15084140

[44] Dong X, Zhang Z, Liu D *et al.* Numerical investigation of the effect of grids and turbulence models on critical heat flux in a vertical pipe. *Front Energy Res* 2018;**6**:58. https://doi.org/10.3389/fenrg.2018.00058

[45] Ivananda D, Ahmad RD, Iswara MAI. Analisis Koefisien Perpindahan Panas Alat Double Pipe Heat Exchanger Berbasis Computational Fluid Dynamics. *DISTILAT J Teknol Separasi* 2023;**9**:240–50. https://doi.org/10.33795/distilat.v9i3.3758

[46] Elankavi S, Shankar U. Study of flow and heat transfer analysis in shell and tube heat exchanger using CFD. *Int Res J Eng Technol* 2008;**5**:468–73. https://doi.org/10.5281/zenodo.3566120

[47] Khan A, Shah I, Gul W *et al.* Numerical and experimental analysis of shell and tube heat exchanger with round and hexagonal tubes. *Energies (Basel)* 2023;**16**:880. https://doi.org/10.3390/en16020880

[48] Dharmalingam R, Sivagnanaprabhu KK, Yogaraja J *et al.* Experimental investigation of heat transfer characteristics of nanofluid using parallel flow, counter flow and shell and tube heat exchanger. *Arch Mech Eng* 2015;**62**:509–22. https://doi.org/10.1515/meceng-2015-0028

[49] Bunaciu AA, Udriştioiu EG, Aboul-Enein HY. X-Ray diffraction: instrumentation and applications. *Crit Rev Anal Chem* 2015;**45**:289–99. https://doi.org/10.1080/10408347.2014.949616

[50] Puspitasari P, Abdullah MMAB, Akhtar MN *et al.* Physicochemical Analysis and Magnetic Properties of Nickel Cobalt Oxide (NiCo2 O 4) Using Self- Combustion Method with Solvent Variation as Supercapacitor Materials. Res Sq., https://doi.org/10.21203/rs.3.rs-2657087/v1, 20 March 2017, preprint: not peer reviewed.

[51] Choudhury BJ, Moholkar VS. Ultrasound-assisted facile one-pot synthesis of ternary MWCNT/MnO2/rGO nanocomposite for high performance supercapacitors with commercial-level mass loadings. *Ultrason Sonochem* 2022;**82**:105896. https://doi.org/10.1016/j.ultsonch.2021.105896

[52] Rasyid A. *Seleksi Material Untuk Casing Sumur Migas & Geothermal*. Jakarta: PT Cipta Gadhing Artha, 2021. 25–7.

[53] Ojrzyńska M, Daniewski AR, Wilczyński K *et al.* High-quality graphene nanoplatelets production with 100% yield based on popular fertilizer industry feedstock. *J Phys Chem C* 2024;**128**:516–24. https://doi.org/10.1021/acs.jpcc.3c06479

[54] Carrillo-Berdugo I, Zorrilla D, Sánchez-Márquez J *et al.* Interface-inspired formulation and molecular-level perspectives on heat conduction and energy storage of nanofluids. *Sci Rep* 2019;**9**:7595. https://doi.org/10.1038/s41598-019-44054-0

[55] Li S, Li Z, Burnett TL *et al.* Nanocomposites of graphene nanoplatelets in natural rubber: microstructure and mechanisms of reinforcement. *J Mater Sci* 2017;**52**:9558–72. https://doi.org/10.1007/s10853-017-1144-0

[56] Taufantri Y, Irdhawati I, Asih IARA. Sintesis dan Karakterisasi Grafena dengan Metode Reduksi Grafit Oksida Menggunakan Pereduksi Zn. *J Kim Val* 2016;**2**:17–23. https://doi.org/10.15408/jkv.v2i1.2233

[57] Mahamude ASF, Harun WSW, Kadirgama K *et al.* Thermal performance of nanomaterial in solar collector: state-of-play for graphene. *J Energy Storage* 2021;**42**:103022. https://doi.org/10.1016/j.est.2021.103022

[58] Bello RH, Coelho LAF, Becker D. Role of chemical funcionalization of carbon nanoparticles in epoxy matrices. *J Compos Mater* 2018;**52**:449–64. https://doi.org/10.1177/0021998317709082

[59] Pang AL, Husin MR, Arsad A *et al.* Effect of graphene nanoplatelets on structural, morphological, thermal, and electrical properties of recycled polypropylene/polyaniline nanocomposites. *J Mater Sci Mater Electron* 2021;**32**:9574–83. https://doi.org/10.1007/s10854-021-05620-3

[60] Kartick B, Srivastava SK, Srivastava I. Green synthesis of graphene. *J Nanosci Nanotechnol* 2013;**13**:4320–4. https://doi.org/10.1166/jnn.2013.7461

[61] Tran VQ, Doan HT, Nguyen NT *et al.* Preparation of graphene nanoplatelets by thermal shock combined with ball milling methods for fabricating flame-retardant polymers. *J Chem* 2019;**2019**:284160. https://doi.org/10.1155/2019/5284160

[62] Alawi OA, Sidik NAC, Kazi SN *et al.* Graphene nanoplatelets and few-layer graphene studies in thermo-physical properties and particle characterization. *J Therm Anal Calorim* 2019;**135**:1081–93. https://doi.org/10.1007/s10973-018-7585-0

[63] Kalsi S, Kumar S, Kumar A *et al.* Thermophysical properties of nanofluids and their potential applications in heat transfer enhancement: a review. *Arab J Chem* 2023;**16**:105272. https://doi.org/10.1016/j.arabjc.2023.105272

[64] Shoghl SN, Jamali J, Moraveji MK. Electrical conductivity, viscosity, and density of different nanofluids: an experimental study. *Exp Therm Fluid Sci* 2016;**74**:339–46. https://doi.org/10.1016/j.expthermflusci.2016.01.004

[65] Elsaid K, Abdelkareem MA, Maghrabie HM *et al.* Thermophysical properties of graphene-based nanofluids. *Int J Thermofluids* 2021;**10**:100073. https://doi.org/10.1016/j.ijft.2021.100073

[66] Atofarati EO, Sharifpur M, Huan Z. Nanofluids for heat transfer enhancement: a holistic analysis of research advances, technological progress and regulations for health and safety. *Cogent Eng* 2024;**11**:2434623. https://doi.org/10.1080/23311916.2024.2434623

[67] Jehhef KA, Siba MAAA. Effect of surfactant addition on the nanofluids properties: a review. *Acta Mech Malaysia*. 2019;**2**:01–19. https://actamechanicamalaysia.com/archives/2amm2019/2amm2019-01-19.pdf

[68] Timofeeva EV, Routbort JL, Singh D. Particle shape effects on thermophysical properties of alumina nanofluids. *J Appl Phys* 2009;**106**:014304. https://doi.org/10.1063/1.3155999

[69] Chhabra RP, Richardson JF. *Non-Newtonian Flow and Applied Rheology: Engineering Applications*. Amsterdam: Elsevier Science, 2017.

[70] Arain AH, Ridha S, Ilyas SU *et al.* Evaluating the influence of graphene nanoplatelets on the performance of invert emulsion drilling fluid in high-temperature wells. *J Pet Explor Prod Technol* 2022;**12**:2467–91. https://doi.org/10.1007/s13202-022-01501-5

[71] Hong WX, Sidik NAC, Saidur R. Effect of surfactants on thermal conductivity of graphene based hybrid nanofluid. *IOP Conf Ser Earth Environ Sci* 2020;**463**:012122. https://doi.org/10.1088/1755-1315/463/1/012122

[72] Nika DL, Balandin AA. Phonons and thermal transport in graphene and graphene-based materials. *Reports Prog Phys* 2017;**80**:036502. https://doi.org/10.1088/1361-6633/80/3/036502

[73] Akbari A, Alavi Fazel SA, Maghsoodi S *et al.* Thermo-physical and stability properties of raw and functionalization of graphene nanoplatelets-based aqueous nanofluids. *J Dispers Sci Technol* 2019;**40**:17–24. https://doi.org/10.1080/01932691.2018.1462713

[74] Pordanjani AH, Aghakhani S, Afrand M *et al.* An updated review on application of nanofluids in heat exchangers for saving energy. *Energy Convers Manag* 2019;**198**:111886. https://doi.org/10.1016/j.enconman.2019.111886

[75] Shojaee S, Mohammad V, Arash ML *et al.* Turbulent flow of a shear-thinning non-Newtonian CMC-based nanofluid in twisted finned tubes with an elliptical profile. *Numer Heat Transf A Appl* 2025;**86**:1860–77. https://doi.org/10.1080/10407782.2023.2282156